J. Phys. B: At. Mol. Opt. Phys. **46** (2013) 145002 (6pp) doi:10.1088/0953-4075/46/14/145002

Auger energies, branching ratios, widths and x-ray rates of double *K*-vacancy states of Ne^{2+}: a close-coupling calculation

Yanpeng Liu, Jiaolong Zeng and Jianmin Yuan

Department of Physics, College of Science, National University of Defense Technology, 410073 Changsha Hunan, People's Republic of China

E-mail: jiaolongzeng@hotmail.com

Received 1 May 2013, in final form 6 June 2013
Published 27 June 2013
Online at stacks.iop.org/JPhysB/46/145002

Abstract

A close-coupling calculation is performed for the photoionization cross section of the high-lying core-excited state $1s2s^22p^5\ ^1P^o$ of Ne^{2+} in the energy region of the double *K*-vacancy resonance $1s^02s^22p^6\ ^1S$. The calculation is carried out by using the *R*-matrix method in the *LS*-coupling scheme, which includes 27 target states and extensive configuration interaction. The $KK-KL$ x-ray energy, rate and autoionization width of the double *K*-vacancy state, together with $KK-KLL$ Auger energies and branching ratios of the main channels, are obtained from the cross sections and the contributions of these channels. The calculated resonance energy and x-ray rate are in good agreement with the existing experimental and theoretical results. For the Auger width, our result agrees well with the available experimental result and it is very close to the average of other theoretical data, which shows considerable differences with each other. The Auger energy of the predominate channel $KK-KL_{23}L_{23}\ ^2D$ is in rather good agreement with recent experiments on the Auger spectra. Our branching ratios for the channels $KK-KL_{23}L_{23}\ ^2D$ and $KK-KL_{23}L_{23}\ ^2S$ are larger than the results obtained by the multi-configuration Dirac–Fock method by ∼20% on average, which may be due to the coupling of the continuum channels.

1. Introduction

The characteristics of the double *K*-vacancy states, known as hollow atoms, have always attracted attention. The newly arisen x-ray free-electron lasers (XFELs) providing very intense femtosecond x-ray pulses were used to investigate the atomic inner-shell processes [1–4]. The production of the hollow states with an XFEL such as the linac coherent light source is accessible since the sequential single-photon absorption became the dominant mechanism [3]. This is quite different from the energetic electrons' impact [5, 6] and the double photoionization of the *K*-shell by absorbing a single photon of the x-ray synchrotron radiation [7, 8]. For low-*Z* atoms such as neon, the double *K*-vacancy states mainly decay by Auger transitions and can be observed by recording $KK-KLL$ Auger electron spectra [3, 5–7]. So the Auger properties including energies, widths and branching ratios are important in modelling the interaction of intense x-ray lasers with atoms, molecules and clusters [9] and in modelling the radiative properties of local thermodynamic equilibrium (LTE) and non-LTE plasmas [10–14]. In addition, Auger rates and branching ratios also play an important role in the investigations of the double Auger decay and the cascade decay from inner-shell vacancy states [15–18].

The Auger transitions of an autoionizing state are entirely due to the electron–electron interactions, and strictly correlated with the coupling of the discrete state and the continuum channels. The close-coupling approximation was used to obtain the properties of the single *K*-vacancy resonances for atoms and ions such as B I [19], O I [20], Ne I [21], Al VII [22], Ne VII [23], Fe XV [24] and the double *K*-vacancy resonances for atomic lithium which has three electrons [25–27]. To our knowledge, few close-coupling calculations were reported for more complex systems with more than three electrons such as $1s^02s^22p^6\ ^1S$ of Ne^{2+}. Some theoretical results were obtained by employing the multi-configuration Dirac–Fock (MCDF) method [6, 28, 29] in the Hartree–Fock (HF) model [30, 31], and some results were obtained in

configuration-average values [29, 30]. Moreover, the autoionization widths in the literature showed considerable differences. However, the effects of coupling between different channels were not included in these MCDF or MCHF methods.

The $1s^02s^22p^6\ ^1S$ resonance can arise from the low-lying state $1s^22s2p^5\ ^1P^o$ of Ne^{2+} via weak double-electron excitation by absorbing a single x-ray photon, just as the experiment for atomic Li [25]. It can also arise from the high-lying core-excited state $1s2s^22p^5\ ^1P^o$ via the single-electron excitation of the K-shell. In the past, the experiment of the latter case was difficult, because the lifetime of the single K-vacancy state is only a few femtoseconds [32]. However, the unprecedented XFELs, which can produce ultra-intense x-rays and make the photoabsorption rate comparable to the Auger rate of the single K-vacancy state, will change this situation [3]. Hence it should be feasible for such photoionization experiments from highly excited states to be carried out. In this work, we calculate the photoionization cross sections of the two initial states mentioned above in the energy region of the $1s^02s^22p^6\ ^1S$ resonance. The calculations are performed in the close-coupling approximation by employing the R-matrix method [33]. Extensive configuration interaction (CI) is taken into account to describe the atomic structure of the target Ne^{3+}. Using the partial cross section of the high-lying state $1s2s^22p^5\ ^1P^o$ and the contributions of the main channels, the resonance energy, the KK–KL x-ray emission rate and the autoionization width of the double K-vacancy state, together with the KK–KLL Auger energies and the branching ratios of the main channels, are determined. Our results are compared with the experimental and theoretical results on the Auger spectra and x-ray spectra.

2. Theoretical methods

The R-matrix method for electron–atom and photon–atom interactions is very effective in considering the resonance structures and was described in great detail by Burke *et al* [34] and Berrington *et al* [35]. The outline of the method is briefly presented in the following, where the LS-coupling is assumed. In the internal region, the basis states ψ_k of the $(N+1)$-electron system are expanded in the form of

$$\psi_k(X_1,\ldots,X_{N+1}) = \hat{A}\sum_{ij} c_{ijk}\Phi_i(X_1,\ldots,X_N\hat{r}_{N+1}\sigma_{N+1}) \times u_{ij}(r_{N+1}) + \sum_j d_{jk}\phi_j(X_1,\ldots,X_{N+1}), \quad (1)$$

where $\hat{A}$ is the antisymmetrization operator for the exchange effects between the target electrons and the $(N+1)$th electron, and i is the channel symbol. X_m stands for the spatial ($\vec{r}_m$) and the spin (σ_m) coordinates of the mth electron. The functions $u_{ij}(r)$ construct the basis sets for the continuum orbitals of the $(N+1)$th electron, and Φ_i are the coupling between the target states and the spin-angle functions of the $(N+1)$th electron to give eigenstates of definite total orbital angular momentum L and total spin S. The quadratically integrable functions ϕ_j are included to ensure the completeness of the total wavefunction. In the external region, the exchange effects between the target electrons and the $(N+1)$th electron have been ignored and the radial functions $F_i(r)$ of the $(N+1)$th electron can be obtained by directly integrating the radial equations. Matching the two regions at the R-matrix radius can complete the solution. The one-electron orbitals of bound states from which the target states and ϕ_j are constructed are represented as linear combinations of the Slater-type orbitals:

$$P_{nl}(r) = \sum_j C_{jnl} r^{I_{jnl}} \exp(-\zeta_{jnl} r), \quad n > l, \quad (2)$$

where the parameters C_{jnl} and ζ_{jnl} are determined by a variational optimization on the energies of the specific LS-coupled states.

This work employs ten orbitals of Ne^{3+}, including five real (1s,2s, 2p, 3s, 3p) and five pseudo-orbitals ($\overline{3d}$, $\overline{4s}$, $\overline{4p}$, $\overline{4d}$, $\overline{4f}$). They are obtained by using the CIV3 code [36] as follows. The orbitals 1s, 2s and 2p are optimized on a linear combination of $1s^22s2p^4\ ^4P$ (92%) and $1s2s^22p^4\ ^2S$ (8%) to take care of the K-shell excited states. The orbitals 3s and 3p are obtained by optimizing on $1s^22s^22p^23s\ ^2S$ and $1s^22s^22p^2(^1S)3p\ ^2P^o$, respectively. The pseudo-orbitals $\overline{3d}$ and $\overline{4d}$ are obtained by optimizing on $1s^22s2p^4\ ^2S$, while $\overline{4p}$, $\overline{4d}$ and $\overline{4f}$ are on $1s^22s2p^4\ ^2P$. The R-matrix radius is chosen to be 9.6 au to ensure that the wavefunctions of bound states are completely wrapped within the R-matrix sphere. As for the construction of the continuum states, the number of the continuum basis functions $u_{ij}(r)$ is set to be 60 to acquire high enough continuum energy.

The main Auger channels from $1s^02s^22p^6\ ^1S$ are

$$\begin{aligned} 1s^02s^22p^6\ ^1S \rightarrow\ & 1s2s^22p^4\ ^2D + kd,\\ & 1s2s^22p^4\ ^2S + ks,\\ & 1s2s2p^5(^3P^o)\ ^2P^o + kp,\\ & 1s2s2p^5(^1P^o)\ ^2P^o + kp,\\ & 1s2p^6\ ^2S + ks; \end{aligned} \quad (3)$$

thus, these five core-excited target states are very important in the close-coupling calculations. The main challenge here is that one has to deal with the highly excited states including both the single- and double-hole (hollow) ones. The energies of single K-vacancy states and the hollow state of $1s^02s^22p^6\ ^1S$ are shown in figure 1 relative to the ground state of Ne^{3+}. The energies of the ground state and $1s^22s2p^5\ ^1P^o$ of Ne^{2+} are taken from the NIST database [37], and their positions are −4.659 Ry and −2.024 Ry, respectively. Energies of K-vacancy states are deduced from the x-ray spectrum [38], except energies of $1s2s^22p^4\ ^2S$, $1s2s2p^5(^3P^o)^2P^o$ and $1s2p^6\ ^2S$, which are the theoretical results in this work. From the inspection of figure 1, one can see that the energies of the single K-vacancy states are higher than the ground state by more than 60 Ry and that of the hollow state by more than 120 Ry.

In this work, 14 lowest terms and 13 core-excited terms of Ne^{3+} are utilized as target states, which are shown in table 1. The 13 core-excited terms belong to configurations of $1s2s^22p^4$, $1s2s2p^5$, $1s2p^6$, $1s2s^22p^33s$ and $1s2s^22p^33p$. In our calculations, the initial term is $1s2s^22p^5\ ^1P^o$ of Ne^{2+} and the final symmetry is ^1S (as we focus on the hollow state of $1s^02s^22p^6\ ^1S$), and therefore some terms of these configurations are irrelevant to our problem and are not included. Firstly, only doublet terms can form possible channels to give the symmetry of ^1S. Secondly, in the doublet

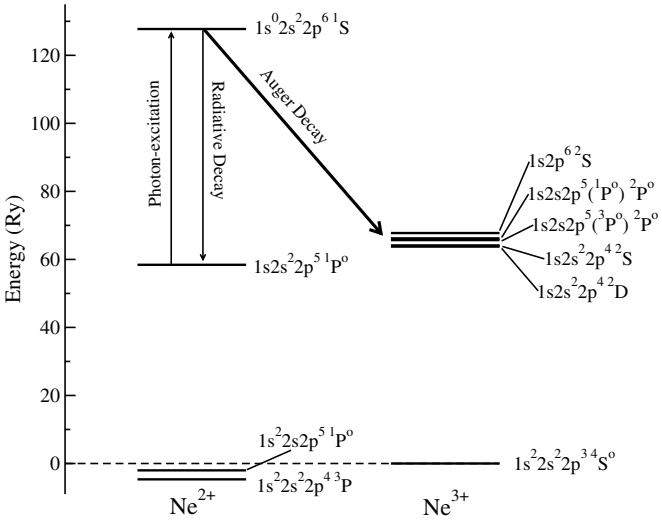

Figure 1. Level structure for the single and double K-vacancy states of Ne^{2+} and Ne^{3+} relevant to this work (relative to the ground state $1s^2 2s^2 2p^3\ ^4S^o$ of Ne^{3+}). Experimental energies are used wherever available.

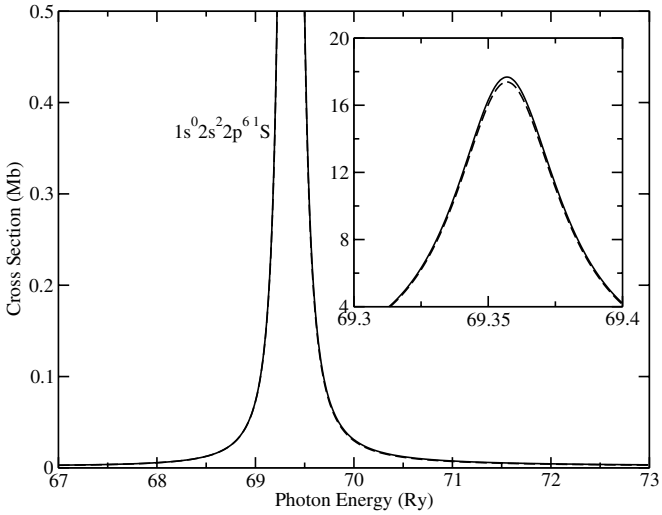

Figure 2. The ^1S partial photoionization cross section of the core-excited state $1s2s^2 2p^5\ ^1P^o$ in the vicinity of the resonance $1s^0 2s^2 2p^6\ ^1S$. The full and dashed lines refer to the length and velocity forms, respectively.

Table 1. Energy levels (in Ry) of the target states of Ne^{3+} and comparison with available NIST data [37]. The values with superscript '$*$' are deduced from the experimental results of the x-ray emission spectrum [38].

Target states	This work	NIST	Diff (%).
$1s^2 2s^2 2p^3\ ^4S^o$	0.000 00	0.000 00	0
$1s^2 2s^2 2p^3\ ^2D^o$	0.380 80	0.375 92	1.30
$1s^2 2s^2 2p^3\ ^2P^o$	0.575 94	0.568 98	1.22
$1s^2 2s2p^4\ ^4P$	1.664 57	1.678 77	0.85
$1s^2 2s2p^4\ ^2D$	2.309 51	2.315 42	0.26
$1s^2 2s2p^4\ ^2S$	2.734 15	2.730 41	0.14
$1s^2 2s2p^4\ ^2P$	2.919 03	2.918 43	0.02
$1s^2 2p^5\ ^2P^o$	4.411 06	4.421 67	0.24
$1s^2 2s^2 2p^2 3s\ ^2D$	4.751 04	4.663 17	1.88
$1s^2 2s^2 2p^2(^3P)3p\ ^2P^o$	4.975 01	4.891 54	1.71
$1s^2 2s^2 2p^2 3s\ ^2S$	5.106 13	4.972 87	2.68
$1s^2 2s^2 2p^2 3p\ ^2F^o$	5.147 40	5.061 14	1.70
$1s^2 2s^2 2p^2(^1D)3p\ ^2P^o$	5.267 98	5.168 35	1.93
$1s^2 2s^2 2p^2(^1S)3p\ ^2P^o$	5.522 71	5.393 24	2.40
$1s2s^2 2p^4\ ^2D$	63.818 13	63.756*	0.10
$1s2s^2 2p^4\ ^2S$	64.121 25		
$1s2s2p^5(^3P^o)\ ^2P^o$	65.678 75		
$1s2s2p^5(^1P^o)\ ^2P^o$	66.139 66	66.191*	0.08
$1s2p^6\ ^2S$	67.757 16		
$1s2s^2 2p^3(^3P^o)3s\ ^2P^o$	68.723 23		
$1s2s^2 2p^3(^3D^o)3p\ ^2D$	68.955 43		
$1s2s^2 2p^3(^1P^o)3s\ ^2P^o$	69.063 62		
$1s2s^2 2p^3(^3P^o)3p\ ^2D$	69.097 42		
$1s2s^2 2p^3(^3P^o)3p\ ^2S$	69.207 13		
$1s2s^2 2p^3(^1D^o)3p\ ^2D$	69.284 94		
$1s2s^2 2p^3(^1P^o)3p\ ^2D$	69.450 85		
$1s2s^2 2p^3(^1P^o)3p\ ^2S$	69.531 00		

terms of $1s2s^2 2p^3 3p$, ^2P, terms cannot couple a free electron to form terms with the ^1S symmetry. Hence, all possible terms from the configurations of $1s2s^2 2p^4$, $1s2s2p^5$, $1s2p^6$, $1s2s^2 2p^3 3s$ and $1s2s^2 2p^3 3p$ which can couple to ^1S terms have been included in our calculation. In principle, one can include more terms such as from the configurations of $1s2s^2 2p^3 3d$, $1s2s^2 2p^3 4s$ and $1s2s2p^4 nl$ (nl = 3s, 3p, 3d) to obtain more accurate results. Yet in this work, 3d is a pseudo-orbital and the energies of the terms of configurations with a 3d orbital are much higher than those included in table 1. Moreover, practical calculations show that the contributions of the terms belonging to the configurations of $1s2s^2 2p^3 3s$ and $1s2s^2 2p^3 3p$ are less than 0.5%. The contributions from $1s2s^2 2p^3 3d$ are comparable with those of $1s2s^2 2p^3 3s$ and $1s2s^2 2p^3 3p$; thus we do not include these terms in the target expansion. The target energies relative to the ground state of Ne^{3+} are listed in table 1 and compared with the NIST data [37]. Values in the last column are the relative differences in percentage. As in figure 1, the two experimental energies of the core-excited states $1s2s^2 2p^4\ ^2D$ and $1s2s2p^5(^1P^o)\ ^2P^o$ are deduced from the experimental results of the high-resolution x-ray emission spectrum [38] and the NIST energies of the final states $1s^2 2s^2 2p^3\ ^2D^o$ and $1s^2 2s2p^4\ ^2P$, respectively. From the comparison, one can see that the relative difference is less than 2.7% for available levels in the NIST database. In particular, it should be noted that the accuracy of the core-excited states is much better than the valence excited states. In this work, two-electron excitations are allowed from the three subshells of the ground configuration and $1s^2 2s2p^4$ of Ne^{3+}, and three-electron excitations are allowed from the three subshells of the ground configuration of the $(N+1)$-electron system.

3. Results and discussions

The ^1S partial photoionization cross section for the high-lying core-excited state $1s2s^2 2p^5\ ^1P^o$ of Ne^{2+} near the region of the double K-vacancy autoionizing resonance $1s^0 2s^2 2p^6\ ^1S$ is displayed in figure 2. Both the length and velocity forms are given and good agreement is found between the two forms. At ~69.36 Ry, a strong resonance appeared, whose peak cross

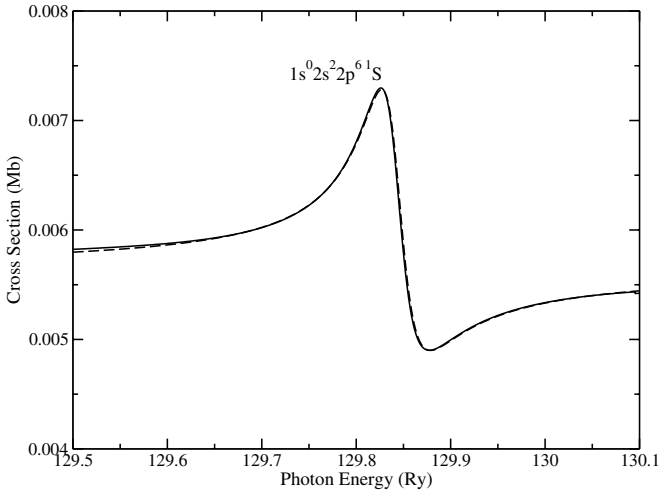

Figure 3. The ^{1}S partial photoionization cross section of the low-lying excited state $1s^2 2s2p^5\ ^1P^o$ in the vicinity of the resonance $1s^0 2s^2 2p^6\ ^1S$ (solid line). The dashed line represents a fitting Fano profile according to (4).

sections are redrawn in the inset. The resonance position and width can be obtained by fitting a Fano profile [39]:

$$\sigma = \sigma_b + \sigma_r \frac{(q+\varepsilon)^2}{1+\varepsilon^2}, \tag{4}$$

where σ_b and σ_r stand for the constants related to the background and the resonance cross sections, respectively. $\varepsilon = 2(E - E_r)/\Gamma$, with E being the photon energy, E_r the resonance energy and Γ the autoionization width, and the parameter q describes the shape of the resonance. According to equation (4), the resonance energy is determined to be 69.357 Ry and the width is 0.0478 Ry.

The resonance width can also be deduced from the ^{1}S partial photoionization cross section of the low-lying excited state $1s^2 2s2p^5\ ^1P^o$ in the vicinity of the double K-vacancy resonance, as the solid line in figure 3 shows (length form). The dashed line represents a fitting Fano profile by equation (4), where the width is also 0.0478 Ry, and the resonance energy and the parameter q are 129.843 Ry and -1.49, respectively. The same width value of 0.0478 Ry is thus obtained from the cross sections for different initial states. This is an important consistency check on our calculation. In the resonance region, the cross section is less than 0.008 Mb, while the continuum background is about 0.005 Mb. It means that the double-electron transition from $1s^2 2s2p^5\ ^1P^o$ to $1s^0 2s^2 2p^6\ ^1S$ is very weak. Near the resonance energy, there is a strong asymmetry for the Fano profile, meaning that there is strong interference between the direct and indirect photoionization channels.

Since the photoionization cross section and the differential oscillator strength $\frac{df}{d\epsilon}$ satisfy $\sigma = 4\pi^2 \alpha a_0^2 \frac{df}{d\epsilon}$, the resonance absorption oscillator strength can be obtained from the photoionization cross section

$$f(L_i S_i \to L_j S_j) = \frac{1}{4\pi^2 \alpha a_0^2} \int_{\Omega_{E_r}} \sigma(\epsilon; L_i S_i \to L_j S_j)\, d\epsilon, \tag{5}$$

where α and a_0 are the fine-structure constant and the Bohr radius, respectively, ϵ is in Ry, and Ω_{E_r} is a region including the resonance transition energy E_r at the centre. L_i,S_i,L_j,S_j are the total orbital and spin angular momenta of the initial bound terms and the final continuum states, respectively. From figure 2, we can see that the background cross section is very small; thus the contribution of the continuum background cross section is negligible compared with that of the resonance. The length and velocity forms of the absorption oscillator strength are determined to be 0.166 and 0.163, respectively. The spontaneous radiative rate from $1s^0 2s^2 2p^6\ ^1S$ to $1s2s^2 2p^5\ ^1P^o$, which is the hypersatellite of the K_α transition (K_α^h), can be obtained by

$$A_{L_j S_j \to L_i S_i} = 8.0324 \times 10^9 s^{-1} E_r^2 \frac{g_i}{g_j} f(L_i S_i \to L_j S_j), \tag{6}$$

where E_r is in Ry, g_i and g_j are the weights of the initial bound and the final autoionizing states, respectively.

Table 2. K_α^h x-ray energy E_r (Ry), rate A_{ji} (10^{13} s^{-1}) and autoionization width Γ_a (eV) of the double K-vacancy state $1s^0 2s^2 2p^6\ ^1S$. Available experimental and theoretical data are given for comparison.

	Experiment	This work	Other theory
E_r	69.279[a], 69.338[b]	69.357	69.485[c], 69.335[d], 69.338[e], 69.317[f]
A_{ji}		1.924	1.951[c], 2.02[d], 3.09[e], 2.012[f]
Γ_a		0.650	0.707[c], 0.513[d], 0.804[e], 0.595[f], 0.623[g]

[a][38], [b][40], [c][30], [d][31], [e][28], [f][29], [g][6].

In table 2, the K_α^h x-ray energy, rate and the autoionization width of the double K-vacancy state are compared to experimental and other theoretical results. Energies from different theoretical results are close to the experimental value of 69.338 Ry [40], and the maximal difference of 0.147 Ry is due to an early research using the Hartree–Fock–Slater model with Herman–Skillman wavefunctions [30]. The K_α^h x-ray rates agreed with each other within a relative difference of less than 5%, except for the result presented by Chen [28]. From the inspection of table 2, it can be seen that there is a discrepancy for the theoretical autoionization widths, even for the calculations using the same method. This might be due to the different wavefunctions used in different calculations. The width of 0.623 eV was obtained with wavefunctions in the initial state frozen orbital approximation [6] and the width of 0.595 eV was deduced by modified Auger electron radial matrix elements of the single K-vacancy state [29], while the width of 0.804 eV was calculated with a wavefunction of the initial state in the single-configuration approximation and wavefunctions of the final states being evaluated in an average-level scheme [28]. The result of 0.513 eV was calculated in the intermediate-coupling scheme using the HF atomic model [31]. Our result 0.650 eV is very close to the average value (0.6484 eV) of these theoretical data. To the best of our knowledge, the only experimental result available in the literature was the measured total width of the Auger transition $1s^0 2s^2 2p^6\ ^1S \to 1s2s^2 2p^4\ ^2D + kd$ (1.0 ± 0.1 eV) obtained by analysing the Auger electron spectrum [7]. The nature width of $1s^0 2s^2 2p^6\ ^1S$ is the sum of the autoionization width Γ_a and the radiative width (0.013 eV) calculated from the x-ray rate A_{ji}. Considering the natural width of both $1s^0 2s^2 2p^6\ ^1S$ (0.663 eV) and $1s2s^2 2p^4\ ^2D$ (0.27 eV) [32], the total width is 0.933 eV, which is in good agreement with the experiment.

Table 3. Auger energies E_a (in Ry) and branching ratios (BR in %) of the channels shown in figure 4. Available experimental and theoretical data are given for comparison.

	Experiment	This work		Other theory	
Channels	E_a	E_a	BR	E_a	BR
$1s2s^22p^4\ ^2D + kd$	63.980[a,b]	63.987	66.16	64.120[c], 64.105[d]	61.26[c], 49.2[d]
$1s2s^22p^4\ ^2S + ks$		63.684	9.96	63.855[c], 63.848[d]	6.89[c], 9.2[d]
$1s2s2p^5(^3P^o)\ ^2P^o + kp$		62.126	2.19	62.040[c], 62.054[d]	0.41[c], 1.1[d]
$1s2s2p^5(^1P^o)\ ^2P^o + kp$		61.665	18.11	61.518[c], 61.525[d]	26.14[c], 33.0[d]
$1s2p^6\ ^2S + ks$		60.048	3.19	59.725[c], 59.747[d]	5.84[c], 7.0[d]
$1s2s^22p^3(^3P^o)3s\ ^2P^o + kp$		59.082	0.10		
$1s2s^22p^3(^1D^o)3p\ ^2D + kd$		58.520	0.18		
$1s2s^22p^3(^1P^o)3p\ ^2D + kd$		58.354	0.06		

[a] [6], the uncertainty was 0.022 Ry.
[b] [7], the uncertainty was 0.002 Ry.
[c] [28], MCDF, initial state in single configuration, final states in average-level scheme.
[d] [6], MCDF, initial state frozen orbital approximation.

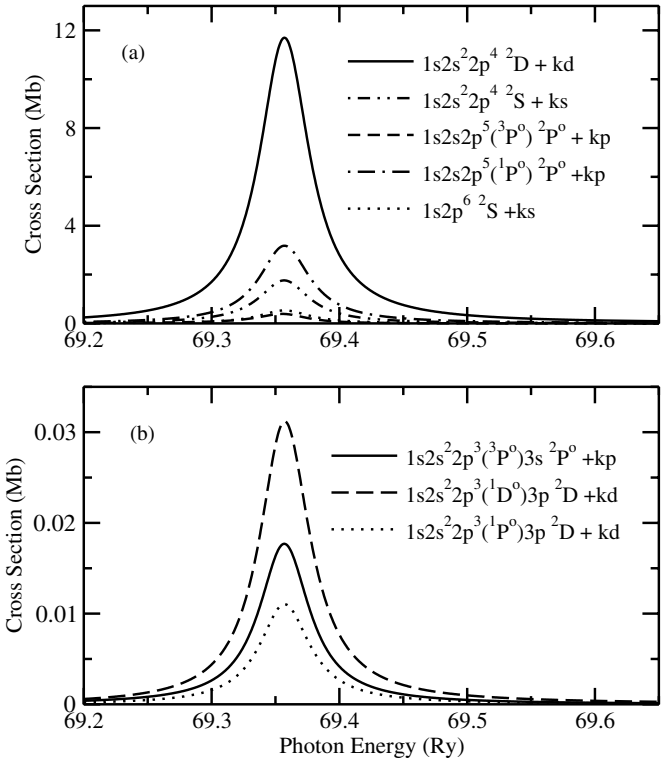

Figure 4. Contributions of continuum channels to the ^1S partial cross section of $1s2s^22p^5\ ^1P^o$ in the vicinity of the resonance $1s^02s^22p^6\ ^1S$ from (a) the main five channels listed in (3) and (b) three shake channels.

Contributions of the main channels to the partial cross section are displayed in figure 4(a), and contributions of three shake channels are displayed in figure 4(b). Only the length form is presented as the results of velocity form are very close to that of the length form. From the inspection of figure 4, it can be seen that $1s2s^22p^4\ ^2D + kd$ is by far the dominant channel of the Auger transition from $1s^02s^22p^6\ ^1S$, accounting for ∼65% of the total cross section. Contributions of $1s2s2p^5(^1P^o)\ ^2P^o + kp$ and $1s2s^22p^4\ ^2S + ks$ are the second and third largest channels, respectively. The contribution from the shake channels in figure 4(b) is tiny compared to the main channels given in figure 4(a), and they contribute less than 0.4% to the total cross section. Auger energies and branching ratios of these channels are listed in table 3. In this work, the energy positions of the initial states $1s2s^22p^5\ ^1P^o$ and $1s^22s2p^5\ ^1P^o$ are 58.448 Ry and −2.038 Ry, respectively. With the resonance energies obtained from figures 2 and 3, the energy position of the double K-vacancy state is calculated to be 127.805 Ry above the ground state of Ne^{3+}, which is very close to the experimental value 127.701 Ry in figure 1. The energies of the Auger electron for these channels are calculated from the energy levels given in table 1. Available experimental and other theoretical results are listed in table 3 as well. The experimental result for the Auger energy of the $1s2s^22p^4\ ^2D + kd$ channel is 63.980 Ry [6, 7] with the uncertainties of 0.022 and 0.002 Ry. Our theoretical Auger energy for this channel is in better agreement with the experiment than the theoretical values obtained by employing the MCDF method [6, 28]. Although the predicted Auger energy is very close for research works [6, 28], the branching ratio differs considerably, meaning the sensitivity of the Auger rates to the wavefunction. Generally speaking, the theoretical Auger energies agree well with each other, yet an evident discrepancy was found for the branching ratio [6, 28]. Such a fact implies that the Auger rate is much more sensitive to the wavefunction. One important aspect for this sensitivity should be the coupling effects of the channels. In R-matrix calculations, the coupling between the discrete states and the continuum channels and the coupling between different continuum channels can be treated in a unified form by using the basis states ψ_k in (1). For example, there is a coupling effect between the continuum channels $1s2s^22p^4\ ^2S + ks$ and $1s2p^6\ ^2S + ks$. With or without the inclusion of such a channel coupling effect will undoubtedly result in a different Auger decay rate.

In conclusion, the ^1S partial photoionization cross section of the high-lying core-excited state $1s2s^22p^5\ ^1P^o$ of Ne^{2+} is calculated in the region of the double K-vacancy resonance. The calculation is performed in a 27-state close-coupling approximation by using the R-matrix method, and extensive CI is taken into account. Using the partial cross section and the contributions of the main channels, the x-ray energy and rate of $1s^02s^22p^6\ ^1S$–$1s2s^22p^5\ ^1P^o$, the autoionization

width of $1s^0 2s^2 2p^6\ ^1S$, and the Auger energies and branching ratios of the main channels, are obtained. Our calculated resonance energy and x-ray rate are in good agreement with the experimental and other theoretical results on the K_α^h x-ray spectra. For the Auger width, available theoretical results in the literature showed considerable differences with each other, and our result is very close to their average value and in good agreement with the available experimental results. The Auger energy of the predominate channel $1s2s^2 2p^4\ ^2D + kd$ is in rather good agreement with recent experiments on the Auger spectra. The branching ratios to different channels are sensitive to wavefunctions and the coupling effects of different channels should be included to obtain reliable results.

Acknowledgments

This work was supported by the National Natural Science Foundation of China under grant nos 11274382, 11274383 and 11204376.

References

[1] Meyer M *et al* 2012 *Phys. Rev. Lett.* **108** 063007
[2] Düsterer S *et al* 2011 *New J. Phys.* **13** 093024
[3] Young L *et al* 2010 *Nature* **466** 09177
[4] Kanter E P *et al* 2011 *Phys. Rev. Lett.* **107** 233001
[5] Šmit Ž, Žitnik M, Avaldi L, Camilloni R, Fainelli E, Mühleisen A and Stefani G 1994 *Phys. Rev.* A **49** 1480
[6] Pelicon P, Čadež I, Žitnik M, Šmit Ž, Dolence S, Mühleisen A and Hall R I 2000 *Phys. Rev.* A **62** 022704
[7] Southworth S H, Kanter E P, Krässig B, Young L, Armen G B, Levin L C, Ederer D L and Chen M H 2003 *Phys. Rev.* A **67** 062712
[8] Hoszowska J *et al* 2009 *Phys. Rev. Lett.* **102** 073006
[9] Xiang W, Gao C, Fu Y, Zeng J and Yuan J 2012 *Phys. Rev.* A **86** 061401
[10] Gao C, Jin F, Zeng J and Yuan J 2013 *New J. Phys.* **15** 015022
[11] Zeng J and Yuan J 2006 *Phys. Rev.* E **74** 025401
[12] Zeng J and Yuan J 2007 *Phys. Rev.* E **76** 026401
[13] Zeng J and Yuan J 2002 *Phys. Rev.* E **66** 016401
[14] Zeng J 2008 *J. Phys. B: At. Mol. Opt. Phys.* **41** 125702
[15] Amusia M Y, Lee I S and Kilin V A 1992 *Phys. Rev.* A **45** 4576
[16] Zeng J, Liu P, Xiang W and Yuan J 2013 *Phys. Rev.* A **87** 033419
[17] Kochur A G, Sukhorukov V L, Dudenko A I and Demekhin Ph V 1995 *J. Phys. B: At. Mol. Opt. Phys.* **28** 387
[18] Kochur A G, Sukhorukov V L and Demekhin V F 2004 *J. Electron Spectrosc. Relat. Phenom.* **137–140** 325
[19] Badnell N R, Petrini D and Stoica S 1997 *J. Phys. B: At. Mol. Opt. Phys.* **30** L665
[20] McLaughlin B M and Kirby K P 1998 *J. Phys. B: At. Mol. Opt. Phys.* **31** 4991
[21] Gorczyca T W 2000 *Phys. Rev.* A **61** 024702
[22] Zeng J, Yuan J and Lu Q 2001 *Phys. Rev.* A **64** 042704
[23] Zeng J and Yuan J 2002 *Phys. Rev.* A **66** 022715
[24] Bautista M A 2000 *J. Phys. B: At. Mol. Opt. Phys.* **33** L419
[25] Cubaynes D *et al* 1996 *Phys. Rev. Lett.* **77** 2194
[26] Zhou H L *et al* 1999 *Phys. Rev.* A **59** 462
[27] Roy A K 2004 *J. Phys. B: At. Mol. Opt. Phys.* **37** 4369
[28] Chen M H 1991 *Phys. Rev.* A **44** 239
[29] Natarajan L 2007 *Phys. Scr.* **75** 47
[30] Bhalla C P, Folland N O and Hein M A 1973 *Phys. Rev.* A **8** 649
[31] Karim K R and Logan L 1999 *J. Quant. Spectrosc. Radiat. Transfer* **61** 659
[32] Schmidt V 1997 *Electron Spectrometry of Atoms using Synchrotron Radiation* (Cambridge: Cambridge University Press)
[33] Berrington K A, Eissner W B and Norrington P H 1995 *Comput. Phys. Commun.* **92** 290
[34] Burke P G, Hibbert A and Robb W D 1971 *J. Phys. B: At. Mol. Phys.* **4** 153
[35] Berrington K A, Burke P G, Butler K, Seaton M J, Storey P J, Taylor K T and Yan Y 1987 *J. Phys. B: At. Mol. Phys.* **20** 6379
[36] Hibbert A 1975 *Comput. Phys. Commun.* **9** 141
[37] Kramida A, Ralchenko Y and Reader J(NIST ASD Team) 2012 *NIST Atomic Spectra Database version 5.0* (Gaithersburg, MD: National Institute of Standards and Technology) (http://physics.nist.gov/asd)
[38] Ågren H, Nordgren J, Selander L, Nordling C and Siegbahn K 1978 *J. Electron Spectrosc. Relat. Phenom.* **14** 27
[39] Fano U 1961 *Phys. Rev.* **124** 1866
[40] Watson R L, Benka O, Parthasaradhi K, Maurer R J and Sanders J M 1983 *J. Phys. B: At. Mol. Phys.* **16** 835